



HAL
open science

Microgel structure-driven linear and non-linear mechanical properties of self-assembled microgel films

Éva Dieuzy, Stéphane Auguste, Kamel Chougrani, Valérie Alard, Laurent Billon, Christophe Derail

► To cite this version:

Éva Dieuzy, Stéphane Auguste, Kamel Chougrani, Valérie Alard, Laurent Billon, et al.. Microgel structure-driven linear and non-linear mechanical properties of self-assembled microgel films. *Colloids and Surfaces A: Physicochemical and Engineering Aspects*, 2021, 613, pp.126082. 10.1016/j.colsurfa.2020.126082 . hal-03126992

HAL Id: hal-03126992

<https://univ-pau.hal.science/hal-03126992>

Submitted on 3 Feb 2023

HAL is a multi-disciplinary open access archive for the deposit and dissemination of scientific research documents, whether they are published or not. The documents may come from teaching and research institutions in France or abroad, or from public or private research centers.

L'archive ouverte pluridisciplinaire **HAL**, est destinée au dépôt et à la diffusion de documents scientifiques de niveau recherche, publiés ou non, émanant des établissements d'enseignement et de recherche français ou étrangers, des laboratoires publics ou privés.



Distributed under a Creative Commons Attribution - NonCommercial 4.0 International License

1
2
3
4
5
6
7
8
9
10
11
12
13
14
15
16
17
18
19

Microgel structure-driven linear and non-linear mechanical properties of self-assembled microgel films

*Eva Dieuzy^{1,2,3}, Stéphane Auguste^{2,4}, Kamel Chougrani⁵, Valérie Alard⁵, Laurent Billon^{1,2,3} *
Christophe Derail^{1,2} **

¹Universite de Pau et Pays de l'Adour, E2S UPPA, CNRS, Institut des Sciences Analytiques & de PhysicoChimie pour l'Environnement & les Matériaux, UMR5254, 64000, Pau, France

²LERAM, LabCom UPPA/URGO, Hélioparc, 2 avenue Angot, 64053 Pau, France

³Bio-inspired Materials group: Functionalities & Self-assembly, E2S UPPA, Hélioparc, 2 avenue Angot, 64053, Pau.

⁴URGO RECHERCHE INNOVATION ET DEVELOPPEMENT ; 42 Rue de Longvic, 21300 Chenôve, France

⁵LVMH Recherche Parfums et Cosmétiques ; 185 Av. De Verdun, 45804 St Jean de Braye, France.

1 **Abstract**

2 Soft self-supported cohesive films were formed by self-assembly of pH- and thermo-
3 responsive P(MEO₂MA-*co*-OEGMA-*co*-MAA) microgels without any preparation and/or
4 post-treatments. Linear and non-linear mechanical properties of those films were
5 characterized respectively by dynamic mechanical measurements at low strain and uniaxial
6 extensional tests at high deformation. A relationship between the microstructure of microgels
7 and the mechanical strength of microgel-based films was successfully established. Compared
8 to microgels crosslinked with Oligo(ethylene glycol) diacrylate (OEGDA), microgels with
9 N,N-methylenebisacrylamide (MBA) demonstrate a less crosslinked structure but especially a
10 looser shell which enables the particles to better interpenetrate between one another and resist
11 to higher deformation. Novel films were also designed by controlled mixing microgels and
12 the synthesis side-product, namely water-soluble polymer, WSP, in a ratio with WSP content
13 till 100%. Those films demonstrated promising mechanical properties due to the structural
14 characteristics of the later. The later act as a lever to tune the elastic modulus of films without
15 diminishing their resistance at strain thanks to its high molar mass and crosslinked structure
16 revealed by Steric Exclusion Chromatography (SEC) measurements.

17

18 Keywords: microgels, particle-based films, dynamic mechanical measurements, linear, non-
19 linear, structure-properties relationship

1 **Introduction**

2 Latexes consist of polymeric particles that are widely used in coating and adhesive
3 applications thanks to their film forming abilities. Upon the simple evaporation of the solvent,
4 the particles self-assemble to form a cohesive and transparent film. The cohesion of structured
5 films is governed by the depth of chain interdiffusion and entanglements between adjacent
6 particles known as coalescence.¹ One of the key requirement to allow chain mobility and
7 promote diffusion is naturally to ensure a temperature well above the glass transition
8 temperature during the film formation process. Yet, the rising interest in structured latex films
9 goes beyond their film forming properties. In addition to the intrinsic properties of the
10 polymer, the particulate structure provides many other parameters to tune according the
11 targeted applications and mechanical properties. Indeed, each particle can be considered as a
12 building block that is tunable in terms of size, structure and morphology. A gradient of
13 crosslinking density within latex particles has demonstrated to greatly impact the mechanical
14 strength of films.^{2,3} In a like manner, blending soft with harder latexes has been extensively
15 studied in view of increasing the film toughness.⁴⁻⁶ Stimuli-responsive microgels, also called
16 “smart nanoparticles” differentiate themselves from classical latex in their high swelling
17 ability that responds to external stimuli such as temperature and pH.⁷⁻¹⁰ Such microgels are
18 widely investigated for their high potential in skincare, cosmetic and biomedical applications.
19 Due to their high swelling and hydrophilic properties, the film formation of microgels is more
20 challenging than latexes and often requires external binding to prevent the redispersion in
21 contact with water. One of the most widespread techniques is known as the Layer-by-Layer
22 assembly and consists of alternating oppositely-charged layers in order to create physical
23 bonds between particles.¹¹⁻¹⁵ Another widespread technique for making dense microgel films
24 is spin coating.¹⁶⁻¹⁸ However, these techniques seem not suitable for skincare applications
25 which require a material spreadable on skin that readily forms a “second skin” film *in situ*. On
26 the other hand, very few studies have reported the self-assembly of microgels into cohesive
27 films without any external (chemical or physical) action. Zhou *et al.*¹⁹ reported the simple
28 formation of (PNIPAM-NMA)-based microgel films by batch precipitation polymerization
29 where the cohesion arose from the self-crosslinking of NMA units. More recently, Sonzogni
30 *et al.*²⁰ designed (PVCL-PBA)-based microgel films on the simple solvent evaporation during
31 which the PBA polymer promoted the chain interdiffusion needed to stabilize the films. The
32 resulting thermoresponsive films exhibit interesting mechanical properties and low
33 cytotoxicity. Along the same line, Boularas *et al.* reported the design of thermoresponsive and
34 transparent P(MEO₂MA-*co*-OEGMA-*co*-MAA) microgel films.²¹ The films were

1 qualitatively described as soft, cohesive and flexible: in sum, promising properties for
2 skincare applications.

3 In a recent study from our group, it was demonstrated that tuning the crosslinker type and the
4 crosslinking density can result in significant structural changes in the microgel
5 microstructure.²² Indeed, the structural analyses revealed that the N,N-
6 methylenebisacrylamide (MBA) crosslinker generates an architecture with a less crosslinked
7 shell and more dangling chains at periphery than with using poly(ethylene glycol) diacrylate
8 (OEGDA) crosslinker.²³ Our group demonstrates that the microstructure in turn greatly
9 influences the rheological properties of concentrated suspensions, especially the capacity of
10 microgels to entangle and interpenetrate between one another.²⁴

11 Taking a step further, the main objective of this paper is to quantify the mechanical
12 strength of the P(MEO₂MA-*co*-OEGMA-*co*-MAA) microgel-based films and understand **to**
13 what extent the microgel microstructure impacts them. Moreover, we propose to pilot
14 mechanical properties with the presence or the addition of a synthesis side-product, the water-
15 soluble polymers.^{22,2520} In this scope, the rheological and mechanical behaviors of
16 P(MEO₂MA-*co*-OEGMA-*co*-MAA) purified microgel films were investigated in both the
17 linear and non-linear domains and the structural deformation under elongation was observed
18 at the microscopic scale using Atomic Force Microscopy. The second objective of the present
19 study was to investigate the origin of the looser microstructure of MBA-crosslinked microgels
20 while the crosslinker contents are set at 2 mol.% in both syntheses. One hypothesis was
21 suggested: MBA crosslinker may react in a greater portion to lead to the synthesis side-
22 products, namely water-soluble polymer chains that did not form finite particles, than with
23 microgels compared to OEGDA crosslinker. The structural characteristics of the water-
24 soluble polymers were analyzed for both MBA and OEGDA syntheses. Finally, the authors
25 explored the properties of novel reformulated films by blending microgels and water-soluble
26 polymers in controlled proportion.

27 **Materials & Methods**

28 **Materials.** Di(ethylene glycol) methyl ether methacrylate (MEO₂MA, 95%), oligo(ethylene
29 glycol) methyl ether methacrylate (OEGMA, terminated by 8 EG units with Mn=475g.mol-
30 1), methacrylic acid (MAA), poly(ethylene glycol) diacrylate (OEGDA, Mn=250 g.mol⁻¹),
31 N,N-methylenebisacrylamide (MBA) and potassium persulfate (KPS) were purchased from
32 Sigma Aldrich and used as received. Purified water from a Millipore Milli-Q system was
33 used.

1 **Microgel synthesis.** The precipitation polymerization of microgels was carried out in a 2 L
2 jacketed glass reactor by following the procedure previously described by Boularas *et al.*^{26,27}
3 Briefly, MEO₂MA (92.6 mmol), OEGMA (10.3 mmol) and varying amounts of crosslinker,
4 either OEGDA or MBA, were dissolved in 930 g of water. The crosslinker ratios were set at 2
5 mol.% *versus* the total vinylic molecules, respectively corresponding to 2.12 mmol. The
6 mixture was introduced in the 2 L reactor and stirring was set at 150 rpm. The reactor was
7 purged with nitrogen for 45 min to remove oxygen at room temperature. MAA (5.41 mmol)
8 was dissolved in 30 g of water and added to the reactor. The mixture was heated to 70°C.
9 Finally, KPS (0.958 mmol) was dissolved in 40 g of water and inserted into the reactor to start
10 the reaction. The reaction was kept at 70°C during 6 hours. At the end of synthesis, the
11 colloidal suspension consists of microgel particles (70 wt%) and water-soluble polymer WSP
12 (30 wt%) which did not fully react to form finite particles.

13

14 **Film preparation.**

15 **Purified films.** To study films formed from the assembly only of microgels, the suspensions
16 are purified through 3 centrifugation cycles of 20 minutes at 20,000 rpm to extract the WSP.
17 Then, films are formed by the straightforward water evaporation of purified solutions at
18 37±5°C in a bell jar oven. Silicone molds are chosen for an easy removal of the dried films.

19 **Blended films.** First, microgel particles and WSP are separated by centrifugation (20 minutes
20 at 20,000 rpm). WSP is kept aside from the first centrifugation cycle whereas microgels
21 receive 3 cycles. Solutions are concentrated by evaporation at about 3 wt.% for practical
22 reasons. Solutions are mixed in controlled proportion and poured in silicone molds. Films are
23 dried like classic microgel films. Five film compositions are compared for each crosslinker
24 type (OEGDA and MBA) from 100 wt.% of microgels (classic purified films) to 100 wt.% of
25 WSP.

26 **Methods**

27 **Atomic Force Microscopy.** Topographic images of the films are captured with a Bruker
28 Multi mode 8 AFM. Peak Force QNM Air mode with ScanAsyst Air probes is chosen to scan
29 films in dry environment. Probes have an average spring constant k of 0.4 N.m⁻¹.

30 **Surface of films:** Films are directly placed onto an AFM stainless-steel disk covered by a
31 double-faced adhesive tape. **Cross-section of films:** Neat cross-sections of thick films are
32 performed with an ultra-cryo microtome apparatus Leica EM UC7, using a cryo-chamber
33 Leica EM FC7 cooled down at -80°C. During surfacing, sample is maintained between two

1 Thermanox coverslips purchased from Thermo Fisher Scientific. **Surface of stretched films:**
2 Films are manually subjected to uniaxial deformation and wrapped around a silicon wafer in
3 their stretched state. Glue is applied on the bottom face of the wafer to maintain deformation
4 but not in contact with the top face. The length between two dots is measured by ImageJ[®], an
5 image analysis software, before and after deformation to calculate the applied strain ϵ .

6 **Rheological and mechanical analyses.** Rheological analyses are performed on a MCR 302
7 rheometer from Anton Paar. The temperature is controlled with the oven chamber by forced
8 dry air stream.

9 **Linear shear measurements** are performed on ≈ 1 mm-thick films with a 8 mm-parallel
10 plates geometry. The linear regime is determined by performing a stress sweep from 0.001 to
11 100% at constant frequency equal to 1 Hz. The linear regime is established by the linearity
12 between stress vs strain and can be assumed that G' has to be in a +/- 10% error margin. The
13 frequency sweeps are carried out from 0.01 to 600 rad.s⁻¹ with constant normal force of 0.2N
14 and under a constant strain which is related to the temperature. Considering the structure of
15 microgels as a continuum with WSP, one can apply the Time-Temperature Superposition
16 (TTS) equivalence. Frequency sweeps are performed from -10°C to 50°C with thermal step of
17 10°C. To ensure the linear regime, strain is set at 1% for temperatures from 50°C to 10°C, at
18 0.1% for 0°C and at 0,01% for -10°C. Master curves were obtained by shifting horizontally
19 the frequency sweeps performed at various temperatures in order to fit the frequency sweep
20 performed at 20°C. The vertical translation is neglected for this low temperature range. Here,
21 the empirical relationship of Williams-Landel-Ferry (WLF) expressed by Eq. (1) does not
22 apply as films are made from crosslinked copolymers.²⁸

23
$$\log(a_T) = - \frac{C_1(T-T_{ref})}{C_2+(T-T_{ref})} \quad (1)$$

24 with C_1 and C_2 empirical constants and T_{ref} the reference temperature. For information only,
25 curves from the logarithmic values of shifting factors as a function of temperature are fitted
26 with the WLF equation. The best fit is obtained for $C_1= 8.86$; and $C_2=101.6$ taking $T_{ref}= 20^\circ\text{C}$.

27 **Extensional rheology at large deformation** is performed by using a SER (Sentmanat
28 Extension Rheometer) geometry which consists of paired windup drums that move in equal
29 but opposite rotation. The geometry doesn't require to clamp the specimen between grips and
30 is particularly appropriate for soft and thin polymer films. Test temperature is varied from
31 20°C to 50°C with no control on the relative humidity. Film dimensions are in the following
32 range: 0.5-1 mm x 1-2 mm x 15-20 mm. Films are extended until rupture with a constant

1 strain rate, also referred to as the Hencky strain rate ϵ_H . The extensional viscosity curves
2 always represent the average from at least five specimens tested in the same condition. Error
3 bars in the Y-axis indicate the standard deviation on the extensional viscosity. The point of
4 rupture corresponds to the average in extensional viscosity but also in time from all the
5 specimens tested. The logarithmic strain, or Hencky strain ϵ_H , is function of $\dot{\epsilon}$ the constant
6 strain rate, t the time, L the sample length at instant t and L_0 the initial sample length as given
7 by equation (2).

$$8 \quad \epsilon_H = \dot{\epsilon} \times t = \ln(L/L_0) \quad (2)$$

9 **Tensile tests** are performed on a texture analyzer TA.XT Plus from Stable Micro Systems at a
10 speed of 1 mm.s^{-1} . Film dimensions are in the following range: $150\text{-}200 \mu\text{m} \times 10 \text{ mm} \times 30$
11 mm . Young's modulus is calculated from the elastic region derived from the first linear slope
12 of the stress-strain curve which here corresponds to strain from 0 and 8%.

13

14 **Steric Exclusion chromatography (SEC)** apparatus consists of a set of aqueous columns
15 from Shodex and an Agilent 1260 Iso pump from Agilent technologies. The set-up is further
16 described elsewhere.²⁹ The apparatus is coupled with a Multi Angle Light Scattering (MALS)
17 and a differential refractometer detector (RI). The MALS detector is a Dawn Heleos detector
18 from WYATT Technology. The RI detector is an Optilab T-rEX from WYATT Technology
19 operating at a laser wavelength of 664 nm. During the experiment, the flow rate is set on 0.5
20 mL/min and the column temperature is fixed at 30°C . The mobile phase consists of an
21 aqueous solution of NaNO_3 at 0.1 g.mol^{-1} (8.2 g.L^{-1}), and azide sodium NaN_3 (0.1 g.L^{-1}) as
22 eluent, stabilized with a buffer at pH 8. Before use, the mobile phase is filtered at $0.1 \mu\text{m}$. The
23 solutions of water-soluble polymers are prepared at a concentration of 500 ppm in a buffer of
24 pH 8, from which a volume of $100 \mu\text{L}$ is injected. Before use, the solutions are filtered at 250
25 nm to remove any impurities and eventual microgels. Data were analyzed by using a Zimm
26 model on Astra 6.1 software. The detection limit of the equipment for the radius of gyration is
27 $\approx 10 \text{ nm}$.

28

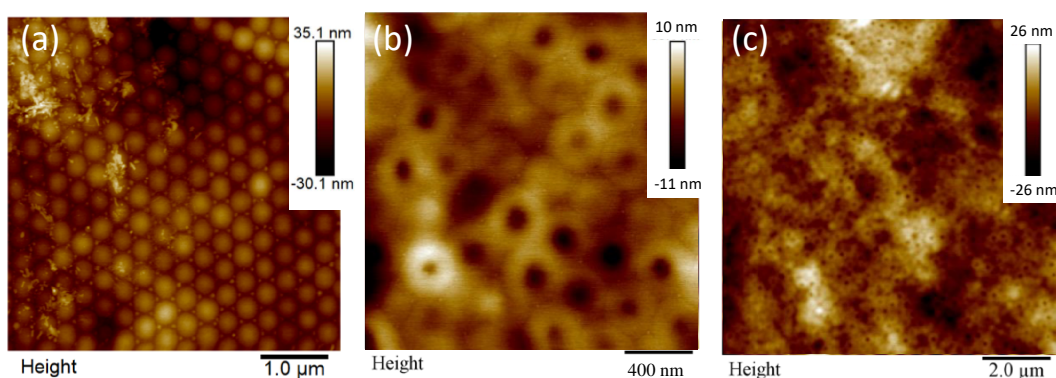
29 **Results and Discussion**

30 OligoEthyleneGlycol microgels were synthesized as previously described by our group.^{22,26}
31 Indeed, such OEG-based microgels were described to present the interesting property to be
32 self-assembled *via* simple solvent evaporation process at surface skin temperature and
33 ambient pressure. They spontaneously form a self-assembled and self-supported transparent

1 film without any external triggers or post-reactions.²¹ Herein, two different approaches were
2 developed based on purified microgels and reformulated microgels with various wt% of WSP.
3

4 **Microstructure of purified microgels films**

5 Height mappings were performed by AFM on the top surface as well as on cross section of
6 microgel films in order to study the self-assembly of microgels. Figure 1 (a) shows a mapping
7 of top surface of 2-MBA crosslinked films whereas Figure 1 (b) and (c) show the mapping of
8 the cross-section of 2-MBA films. Corresponding AFM mappings of OEGDA-crosslinked
9 films are found in Figure S1.



10

11 **Figure 1.** AFM height mappings of microgel films crosslinked with 2 mol.% MBA (a) 5μm x
12 5μm scan of top surface (b) 2μm x 2μm scan of cross section (c) 10μm x 10μm scan of cross-
13 section. Corresponding AFM mappings for OEGDA-crosslinked films are shown in SI.

14 It is observed from Figure 1 (a) that the top layer of microgel particles self-assembles into a
15 perfect hexagonal-close-packed *hcp* array. One can observe from the three images that the
16 particles do not significantly coalesce and keep their spherical shape. Yet, the images reveal a
17 continuous phase around the lighter part that is comparable to a matrix. One can assume that
18 the soft and loosely crosslinked shells of microgels have inter-diffused between one another
19 to form this continuous phase whereas the lighter, *i.e.* higher parts corresponds to the more
20 crosslinked part of microgels, *i.e.* the core. One can observe from Figure 1 (b) and (c), which
21 correspond to the bulk of the film, a more disordered assembly through the thickness of the
22 film but with some evidence for a *hcp* array in the entire thickness of the films. A height
23 difference of ≈ 15 nm between core and shell is also observed showing a “donuts” shape. This
24 “donuts” shape could arise from the presence of water molecules non-homogenously
25 distributed within the microgels due to the core-shell structure. As one knows, microgel films

1 contain and absorb water from their environment due to their hydrophilic properties and low
2 glass transition temperature OEG-based microgels, especially. Indeed, Aguirre *et al.*
3 described after drying of the films, the presence of some water molecules (~15 wt% by TGA
4 measurements) due to the spontaneous wet adsorption from air.²⁵ In particular, the passage
5 from the cryo microtomy sectioning at -80°C back to room temperature certainly makes them
6 gain a significant amount of water. Thus, microgels could be swollen in an uneven way due to
7 their non-homogeneous crosslinking distribution. Another hypothesis could be that the dense
8 cores were snatched from the films during cross-sectioning due to their higher rigidity,
9 leading to this “donuts” shape.

11 **Rheological and mechanical behavior of purified microgel films**

12 As established by the pioneering work of Zosel and Ley and supported by many subsequent
13 studies, latex-based films with a particulate crosslinked structure commonly exhibit a
14 viscoelastic response similar to continuously crosslinked films due to the presence of partial
15 chain inter-diffusion across particle boundaries.^{30–33} As a consequence, some basic concepts
16 from homogenous networks can be applied such as the time-temperature superposition (TTS)
17 principle which allows to access broader frequency ranges.^{28,34} Hence, dynamic mechanical
18 behavior in the linear regime of purified microgel films was explored through frequency
19 sweeps at several temperatures. Master curves built at 20°C for purified microgel film
20 crosslinked with 2 mol. % of MBA and 2 mol.% of OEGDA are respectively shown in Figure
21 2 A and B. The logarithmic values of the TTS shifting factors a_T *versus* temperature are
22 inserted in Figure 2 (A) and (B).

23 By reaching higher frequencies, the master curve allows to observe the transition from the
24 rubber plateau to the glassy region. The glass transition is indicated by two crossover points
25 of G' and G'' which are located respectively at about 10 rad.s⁻¹ and 3x10³ rad.s⁻¹ for both
26 crosslinkers. This finding points out that the glass transition occurs at the same frequency, or
27 equivalently at the same temperature, regardless of crosslinker type. It was expected as the
28 crosslinker remains in very small proportion (2 mol.%) compared to polymer content.

29 The master curve also refines the value of G' at the rubber plateau by reaching lower
30 frequencies. The typical $G'-G''$ cross-over indicating the transition from the rubber plateau to
31 the flow region for thermoplastic polymers is not observed in this range. The absence of flow
32 may reveal that there are no disentanglements of polymer chains at the scale of the particle

1 neither disentanglements between microgels. While no disentanglement within microgel
 2 particle is expected due to crosslink points, the absence of slippage between microgels can be
 3 explained by some strong physical entanglements of chains between neighboring particles. As
 4 reported by many studies on particle-based latex films, dynamic mechanical measurements at
 5 low strain do not differentiate particulate networks from homogenous networks when exists
 6 the presence of partial chain inter-diffusion across the particle boundaries.^{30,31} Nonetheless,
 7 one can suggest the flow region might have been visible by accessing even lower frequency.
 8 Yet, lower frequency means higher temperature which would have led to the change in
 9 microstructure as well a considerable loss of water from these temperature-dependent and
 10 highly hygroscopic microgels presenting a VPTT transition.^{22,26,27} From the reading of the
 11 master curves, the storage moduli at the rubber plateau (10^{-3} rad.s⁻¹) are about $6 \cdot 10^4$ Pa and
 12 $9 \cdot 10^4$ Pa for OEGDA and MBA films, respectively. Since these microgel films are
 13 hygroscopic and the relative humidity rates during the tests cannot be controlled, the standard
 14 deviation has been assessed on films with different storage times and films casted from
 15 different microgel syntheses (Table 1).

16 Although OEGDA films seem to exhibit higher values of G' and G'' than MBA ones, yet the
 17 difference seems to be non-significant considering the relative large standard deviation. In
 18 conclusion, one can note that the two systems exhibit very similar dynamic rheological
 19 responses and the crosslinker type does not induce significant differences in the linear regime.
 20 Both microgel-based films behave as a continuously crosslinked film in spite of their
 21 particulate structure of self-assembled soft colloid spheres.

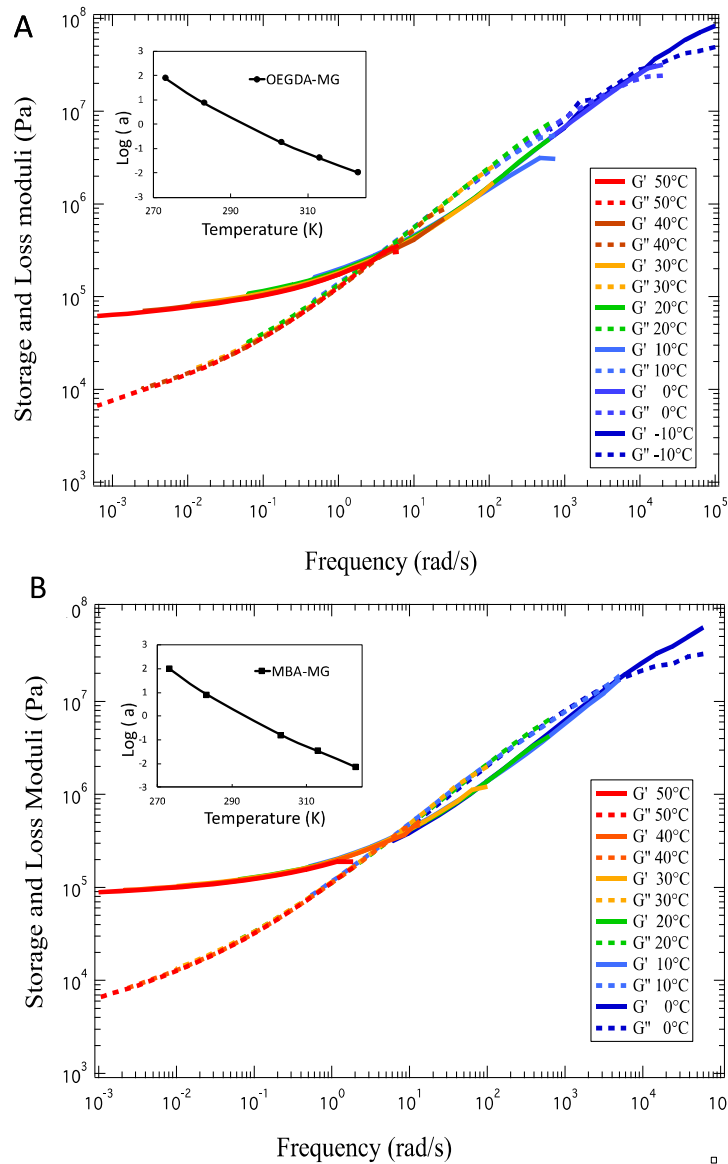
22

23 **Table 1.** Storage and loss moduli for purified P(MEO₂MA-co-OEGMA-co-MAA) microgel
 24 films crosslinked with 2 mol.% MBA and 2 mol.% OEGDA.

	2 mol.% OEGDA	2 mol.% MBA
G' (*10 ⁴ Pa)	8 ± 4	4 ± 2
G'' (*10 ⁴ Pa)	1.1 ± 0.5	0.6 ± 0.2

25

26



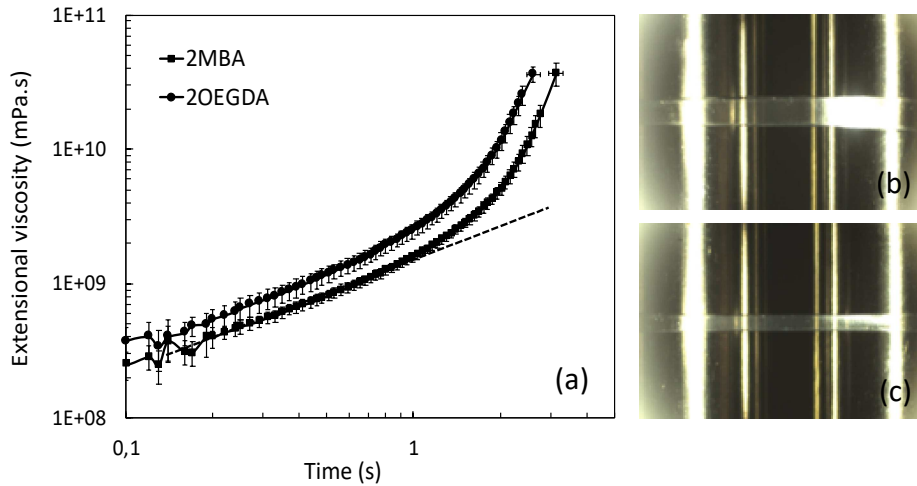
1

2 **Figure 2.** Master curves at $T_{\text{ref}}=20^\circ\text{C}$. Storage modulus G' (solid line) and loss modulus G''
 3 (dashed line) *versus* frequency for purified microgel films crosslinked with (A) 2 mol.%
 4 OEGDA (B) 2 mol.% MBA. The temperature-dependency of the logarithmic shifting factors
 5 are inserted in the graph of the corresponding sample.

6

7 Dynamic mechanical measurements were complemented with uniaxial tests as the later can
 8 generate a much higher degree of molecular orientation than simple shear in the linear
 9 domain. Thus, it can bring additional information regarding the chain disentanglement and
 10 may differentiate the two types of films. Extensional rheology represents one type of uniaxial
 11 elongation tests during which the specimen is pulled at a constant Hencky strain rate $\dot{\epsilon}$
 12 contrary to traditional tensile tests where the crosshead speed is set constant.³⁵ The average

1 extensional viscosity *versus* time for OEGDA and MBA-crosslinked microgel films are
 2 reported in Figure 3 (a) for a Hencky strain rate of 0.5 s^{-1} at 20°C . Figure 3 (b) and (c)
 3 respectively show a film at rest before test and in its stretched state just before the rupture on
 4 the SER geometry.



5
 6 **Figure 3.** Average extensional viscosity *versus* time of purified P(MEO₂MA-*co*-OEGMA-*co*-
 7 MAA) microgel films crosslinked with 2 mol.% OEGDA and 2 mol.% MBA at 20°C . Strain
 8 rate was set at 0.5 s^{-1} . Dashed line represents the linear viscoelastic response described by
 9 $\eta_E = 3x \eta^*$. Film before the test (b) and just before the rupture (c).

10 For both systems, the extensional viscosity steadily increases at first following the linear
 11 viscoelastic response that relates the extensional viscosity η_E to the complex shear viscosity
 12 η^* as given by Eq. (3). The multiplicative constant, referred to as the Trouton ratio Tr is set at
 13 3 for extensional flow. The linear response from Eq. (3) is represented by the dashed line in
 14 Figure 3.

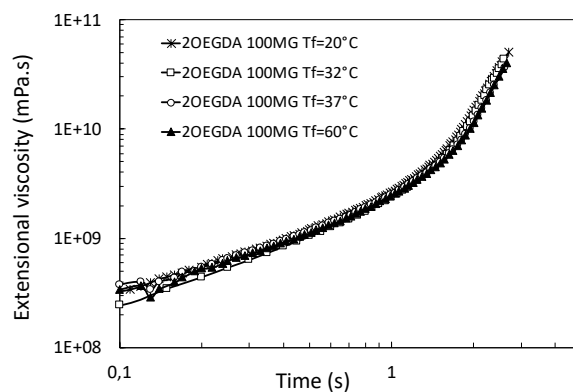
$$15 \quad \eta_E = Tr \times \eta^* = 3x \eta^* \quad (3)$$

16 MBA films exhibit lower values of extensional viscosity than OEGDA ones. It may be
 17 explained by lower values of G' and G'' measured in the linear regime for MBA films (Table
 18 S1). At Hencky strains greater than 0.5, or equivalently time superior to 1 s, the experimental
 19 extensional viscosity deviates and increases faster than the linear response. This upward
 20 deviation is referred to the so-called strain-hardening and commonly occurs in chemically
 21 crosslinked as well as branched polymers. It is characteristic of the chain-branching
 22 architecture as well described in the literature.³⁶⁻⁴⁰ The chain entanglements start to resist to

1 extension whenever the limit of chain extensibility is approached and cause the stiffening of
2 the network. As a result, the extensional viscosity follows a rapid upward increment with
3 elongational time. Herein, strain-hardening is suspected to be caused by both the crosslinked
4 points within microgels and the strong physical entanglements between neighboring microgel
5 particles. The strain at rupture was calculated by multiplying the time at rupture by the strain
6 rate used, Eq. (2). Contrary to the small amplitude oscillatory shear measurements, a
7 significant difference emerges from the two crosslinkers used in the non-linear deformation
8 domain. Indeed, MBA films break at $157 \pm 9 \%$ whereas OEGDA ones break at $131 \pm 7\%$.
9 Aside, the use of different Hencky strain rates (1, 0.5 and 0.1 s^{-1}) seems to not influence on
10 the strain at rupture as observed in Table S1.

11 The network of MBA-crosslinked microgels demonstrates a higher resistance to stress
12 compared to OEGDA ones. This finding echoes the results recently reported by our group on
13 these systems in their suspension form.²³ Indeed, the structural analyses revealed that MBA
14 crosslinker generates an architecture that is more suitable for interpenetration between
15 particles namely a less crosslinked shell and more dangling chains. As a consequence,
16 concentrated suspensions of MBA microgels developed a much higher yield stress than
17 OEGDA ones due to better chain entanglements between close packed particles. In like
18 manner, once films are formed, MBA-crosslinked microgels are better entangled between one
19 another at their interfaces which results in higher strains at rupture.

20 In addition, the impact of the temperature of formation was assessed for films formed at 20°C ,
21 32°C , 37°C and 60°C (Figure 4). Indeed, microgels immersed in aqueous solvent can either
22 be swollen or collapsed due to their thermoresponsive property, *i.e.* the VPTT. The objective
23 was to evaluate whether the state of microgels impacts the quality of the assembly during the
24 film formation, *i.e.* whether swollen microgels inter-diffuse more between neighboring
25 particles than collapsed particles.



1
 2 **Figure 4.** Extensional viscosity *versus* time of 2-OEGDA microgel film tested at 20°C with
 3 Hencky strain of 0.5 s⁻¹. Films were formed at different temperatures: 20°C, 32°C, 37°C and
 4 60°C.

5 The temperature of formation has clearly no impact on the extensional viscosity neither the
 6 strain at rupture. Whether the microgel films are formed under (20°C), within (32°C, 37°C) or
 7 above the VPTT (60°C), the Hencky strain at rupture remains equal to 133 ± 2 %. The
 8 polymer chains may keep some mobility at 60°C which enable the microgels to interpenetrate
 9 between each other in their collapsed state. Indeed, it was previously described in other
 10 studies that microgels still contain a non-negligible content of water when they are in their
 11 collapse state.^{9,41,42} The water is essentially located in the shell providing mobility to the
 12 external dangling chains which are the main responsible for the inter-diffusion. In addition,
 13 microgel films are stored and tested at room temperature, without control of hygrometry, once
 14 formed. Chains may have time to relax and inter-diffuse at microgel boundary thanks to their
 15 solid-like viscoelastic behavior.

16 Uniaxial tensile tests were performed and compared to the extensional viscosity
 17 measurements. The stress *versus* strain curves for OEGDA and MBA-crosslinked microgel
 18 films are reported in Figure 5. **Young's modulus**, the tensile strength (equivalent to the tensile
 19 stress at break in this case), the strain at break and the fracture energy were extrapolated from
 20 the curves (Table S2).

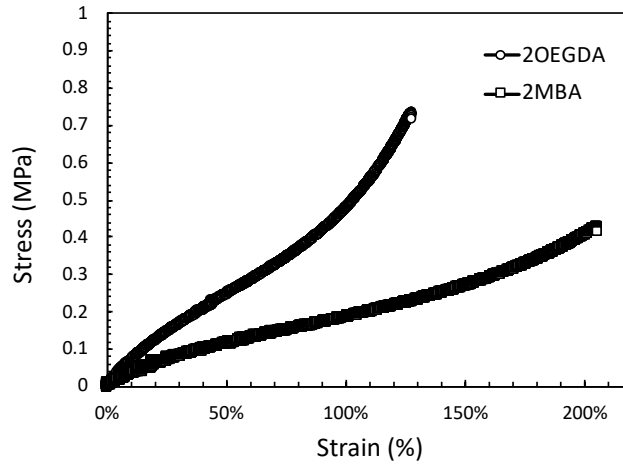


Figure 5. Stress-strain curves of OEGDA and MBA-crosslinked microgel films performed at a crosshead speed of $1\text{mm}\cdot\text{s}^{-1}$ at 20°C .

The tensile behavior of both films is characteristic of elastomers, *i.e.* polymers that exhibit a rubber-like elasticity and require a high force to break, principally due to strain-hardening.⁴³ Similarly to extensional viscosity, strain hardening arises from the resistance to polymer chain alignment. It is clearly observed that MBA films are definitely softer than OEGDA films which results in a lower Young's modulus and lower tensile strength. It corroborates with the lower extensional viscosity values and the lower shear modulus measured in the linear regime. In agreement with the extensional viscosity, MBA films exhibit a much higher elongation at break than OEGDA ones at $201 \pm 24\%$ and $127 \pm 15\%$, respectively. The fracture energy *i.e.* the toughness of MBA films is identical to OEGDA films ($0.39\text{ MJ}\cdot\text{m}^{-3}$) which arises from the opposite effects of a lower tensile stress but a higher strain at break. The Hencky elongations at break from the extensional viscosity measurements were converted to engineering strain with Eq. (5) to be compared with the tensile elongations at break.

$$e = \exp(\varepsilon_H) - 1 \quad (5)$$

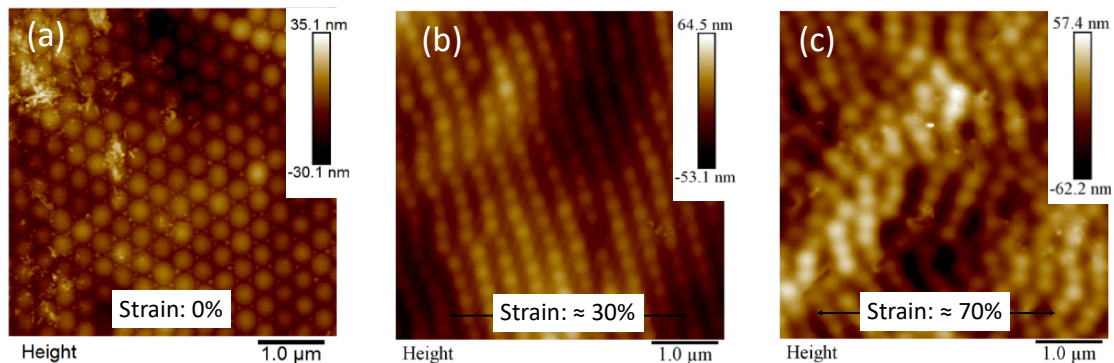
where e is the engineering strain defined by the change in length ΔL per unit of the initial length L_0 .

The converted engineering strains at break from extensional viscosity are 270% and 395% for OEGDA and MBA films, respectively. These values are much higher than the tensile strains. The discrepancy can be attributed to the tensile geometry that is less suitable for soft and thin polymers. The jaws firmly squeeze the thin films which often leads to a premature fracture

1 located below the grips and not ideally at the middle of the specimen. This observation
2 confirms that the elongational properties of soft and viscoelastic films were preferentially
3 evaluated by extensional viscosity thereafter.

4 Young's moduli and tensile strengths of these films are relatively low compared to the ones
5 reported in the literature for other free-standing microgel films elaborated without post-
6 crosslinking techniques.^{20,44} For instance, Sonzogni *et al.* obtained Young's modulus and
7 tensile strength of 84.2 MPa and 10 MPa respectively for P(VCL-BA) thermoresponsive
8 microgel films.²⁰ Nonetheless, low Young's modulus and tensile strength are desired
9 properties in regard of the potential applications targeted *i.e.* skincare products. Indeed,
10 materials designed for skincare have the paramount requirement to exhibit very similar
11 mechanical properties to the skin ones in terms of elasticity, flexibility and elongation to form
12 an ideal "second skin".⁴⁵⁻⁴⁷ Although the mechanical properties of human skin are subject to a
13 large variability, the values found in the literature for the Young's modulus ranges from 0.01 -
14 2 MPa.⁴⁸ Consequently, Young's moduli measured for these films, between 0.35 MPa and
15 0.65 MPa, are perfectly appropriate for skincare applications. In addition, their elongation at
16 break is much superior to the skin one generally measured below 60%.^{49,50} Hence,
17 P(MEO₂MA-*co*-OEGMA-*co*-MAA) microgel films seems to exhibit very suitable
18 mechanical properties for potential skincare applications.

19 To better understand the arrangement of microgels during deformation, films were observed
20 by AFM in a static stretched state. Figure 6 shows the mappings of MBA films (a) at rest (b)
21 under 30% of strain and (c) under 70% of strain. Similar AFM mappings for stretched
22 OEGDA films are shown in Figure S2.



23

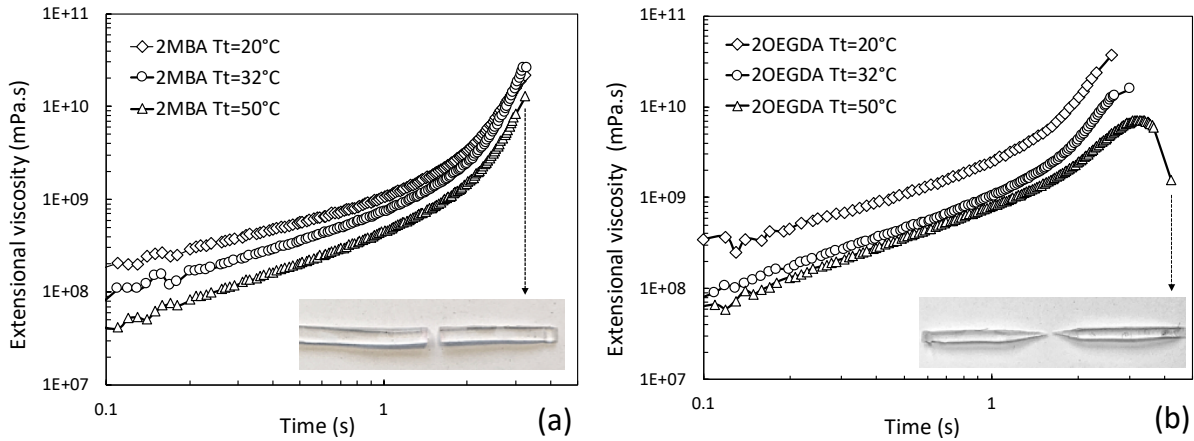
24 **Figure 6.** AFM micrographs performed on MBA-crosslinked films subject to different strains
25 (ϵ): (a) $\epsilon=0\%$, 5 μm scan (b) $\epsilon=30\%$, 5 μm scan (c) $\epsilon=70\%$ 10 μm . The stretching direction is
26 parallel to the X axis of the AFM micrograph.

1 The stretching causes the loss of the hexagonal compact packing of the particle network.
2 Under small deformation ($\varepsilon \approx 30\%$), we observed the alignment of the microgels, more
3 specifically of their cores, in the perpendicular direction of elongation. The distance between
4 two particles is larger than at rest but the cores are not significantly deformed and maintain a
5 spherical shape. It suggests that, at this strain, the deformation mechanism is mostly located at
6 the microgel interface where the entangled chains from the shell stretch to accommodate the
7 stress. Lepizzera *et al.*⁵¹ previously observed a similar deformation pattern on core-shell
8 latexes where the dense core was made from PMMA and the soft shell from P(MMA-*co*-BA-
9 *co*-AA). The authors explained the formation of these “necklaces” from the shrinking of the
10 film width during elongation that pushed the particles closer in the Y direction and further in
11 the X direction. The deformation only occurred in the matrix made from a softer copolymer
12 than the core. Under further elongation ($\varepsilon \approx 70\%$), the structured alignment disappears and is
13 replaced by zig-zags or chevrons (Figure 6c). In addition, cracks are visible by deep gap in the
14 Z direction. The simple deformation of the soft shell is not sufficient anymore to
15 accommodate the stress at large elongation and other deformation mechanisms are at stake.
16 These chevrons and cracks were also observed in the AFM mappings of Lepizzera *et al.*^{51,52}.
17 One can conclude that our systems behave very similarly to composite structured latex films,
18 where the loosely-crosslinked shells represent the soft matrix and the dense cores are
19 comparable to hard fillers.

20 The influence of the test temperature on the film elongational properties has also been
21 evaluated to bring additional knowledge on the chain dynamics at the microgel interface.
22 Figure 7 (a) and (b) respectively show the average extensional viscosity curves of 2-MBA and
23 2-OEGDA films for test temperatures of 20°C, 32°C and 50°C.

24 As an evidence from the relationship between the complex viscosity and the moduli (Eq. (3)
25 and (4)), for both MBA and OEGDA films, one observes that the extensional viscosity is
26 lower at higher temperature.. 2-MBA films exhibit a similar elongation at break at 20°C, 32°C
27 and 50°C corresponding to $\approx 160\%$. The deformation mechanism in the non-linear regime,
28 mostly governed by the stretching of the dangling chains at the microgel interface as observed
29 by AFM, remains identical regardless of the temperature change. Such conclusion cannot be
30 drawn for 2-OEGDA films as observed in Figure 7b. The fracture type evolves from brittle to
31 ductile with the presence of necking at higher temperature (insert in Figure 7b). With the
32 hypothesis of shells from OEGDA microgels being less entangled with one another, one can
33 suggest that the temperature better favors the disentanglements of the chains by slippage at

1 the microgel interface leading to a ductile fracture. In the case of MBA particles, one can
2 suppose that the temperature provided is not sufficient to disentangle the long chains that may
3 have greatly inter-diffused between microgels. Thus, at their maximum elongation, the
4 majority of chains breaks instead of slipping which may result in a brittle fracture.



5
6 **Figure 7.** Extensional viscosity *versus* time of P(MEO2MA-co-OEGMA-co-MAA) microgels
7 crosslinked with (a) 2 mol.% MBA and (b) 2 mol.% OEGDA for different test temperatures:
8 20°C, 32°C and 50°C. Inserted pictures show the films after rupture for $T_{\text{test}}=50^{\circ}\text{C}$.

9 The previous study on purified microgel suspensions as well as the present results on purified
10 films have revealed that microgels crosslinked with 2 mol.% MBA have a lower crosslinking
11 density than OEGDA-crosslinked ones. The looser structure enables a better inter-diffusion of
12 microgels between one another leading to higher yield stress for suspensions and higher strain
13 at rupture for films. In addition, MBA films are softer than OEGDA ones, revealed by the
14 lower elastic modulus. The crosslinking content being set at 2 mol.% in both cases, the author
15 wished to investigate whether a greater portion of crosslinker was reacting with the synthesis
16 side-products *i.e.* water-soluble chains, in the case MBA crosslinking. Structural analyses
17 were then performed on both water-soluble polymers.

18 **Structural characterization of the Water-Soluble Polymer (WSP)**

19 Size Exclusion Chromatography (SEC) measurements coupled with a Multi-Angle Laser
20 Light Scattering (MALLS) detector were performed on OEGDA and MBA-WSP to assess
21 their absolute molecular weight. Measurements were also performed on a linear PEG ($M_w =$
22 35,000 g.mol⁻¹) in order to have a reference of a well-defined linear polymer. Figures S3 (a)
23 and (b) respectively show the molar mass and root-mean-square *rms* radius (or equivalently
24 the gyration radius R_g) as a function of the elution volume.

1 PEG 35K has a weight average molar mass M_w at 34,000 g.mol⁻¹ which validates the
 2 reliability of the method used. As expected, the commercial PEG polymer has a very narrow
 3 distribution with a dispersity value \bar{D} of 1.01. OEGDA and MBA-WSPs have in common a
 4 similar population of molecular masses ranging from 1x10⁴ to 1x10⁵ g.mol⁻¹. Yet MBA-WSP
 5 has a significant proportion of much higher molecular masses ranging from 1x10⁵ to 1x10⁶
 6 g.mol⁻¹. As a result, MBA-WSP has a molar mass of 103,000 g.mol⁻¹ compared to 51,000
 7 g.mol⁻¹ for OEGDA-WSP (Table 2). Conversely to what is reported in some other studies,⁵³
 8 both water-soluble polymers do not correspond to the size of oligomers but to a high
 9 molecular mass polymer.

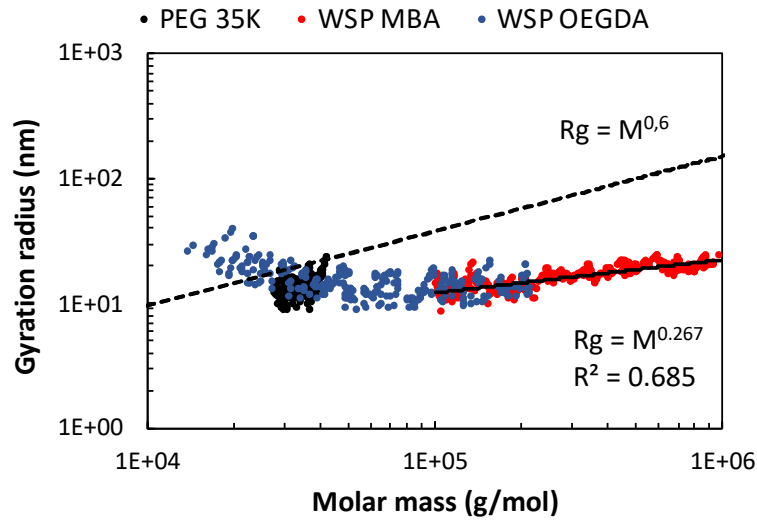
10 **Table 2.** Molecular masses in number (M_n), in weight (M_w) and dispersity index (\bar{D}_M) for
 11 PEG (35,000 g.mol⁻¹), OEGDA-WSP and MBA-WSP for a synthesis with 2 mol.% of
 12 crosslinker

	PEG35K	OEGDA	MBA
M_w (kg.mol ⁻¹)	34	51	103
M_n (kg.mol ⁻¹)	33	34	37
\bar{D}	1.01	1.6	2.8

13
 14 Both WSP exhibit a radius of gyration ≈ 15 nm in average which demonstrates the water-
 15 soluble polymer must have a highly branched and/or crosslinked structure considering their
 16 high molecular masses. The higher molar masses from MBA-WSP reach gyration radii up to
 17 30 nm, indicating bigger but not necessarily denser objects. These results support the idea that
 18 a portion of the crosslinker does not react with the growing microgel particles but creates
 19 water-soluble polymer in solution. In addition, the presence of higher molecular masses for
 20 MBA-WSP reinforces the hypothesis that a higher amount of MBA crosslinker reacts with the
 21 free soluble chains leading to lower crosslinked MBA microgels than OEGDA ones. The
 22 conformational plot, *i.e.* the gyration radius *versus* the molecular weight, is then represented
 23 for OEGDA-WSP, MBA-WSP and PEG 35K (Figure 8). Indeed, the dependence of the
 24 molecular mass with a physical quantity such as the intrinsic viscosity or the radius of
 25 gyration reveals important information on the internal structure, the stiffness and the
 26 branching of macromolecules. The relationship can be described by a power law in a
 27 specified range of molecular weights such as:

28 $R_g \propto M_w^\alpha$ (6)

1 It may be beneficial to recall the theoretical expectation of exponent α for the shape of basic
 2 entities: 0.5 for the random coil conformation of flexible linear polymers in Θ -solvent and
 3 0.33 for spherical particles of uniform density.⁵⁴ A representative power law $R_g \propto M_w^{0.6}$ was
 4 added in Figure 8 to represent a theoretical linear polymer in good solvent.



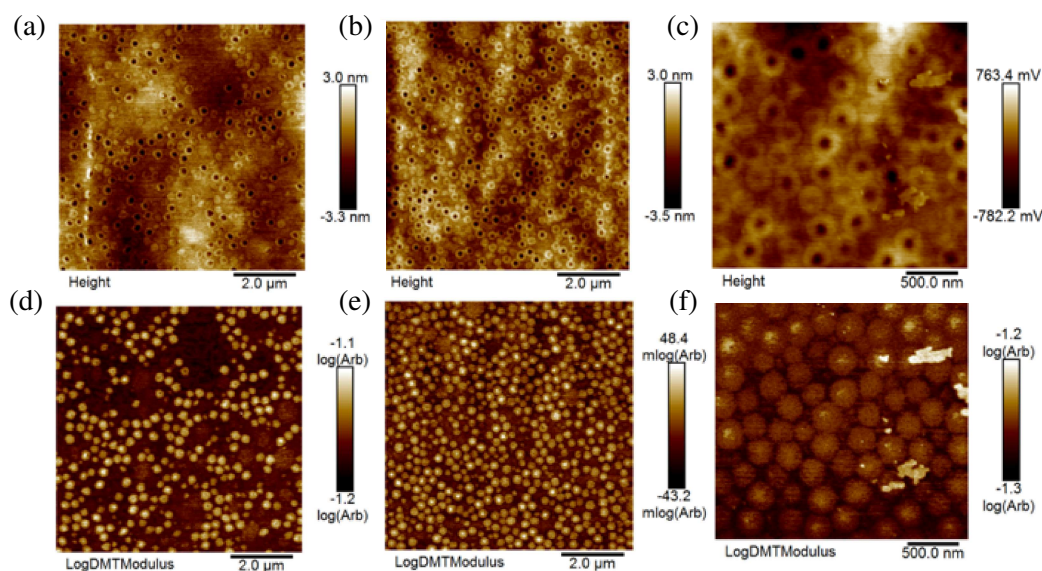
5
 6 **Figure 8.** Conformational plot for (red) MBA-WSP, (blue) OEGDA-WSP, (black) PEG35K.
 7 Dashed line represent the dependence of a theoretical linear polymer with the power law: R_g
 8 $\propto M_w^{0.6}$

9 As previously mentioned, the linear PEG 35K (black dots) has such a narrow distribution in
 10 mass that it is not possible to fit the radius of gyration by a power law. Only MBA-WSP was
 11 fitted by a power law since it is the population with the clearest and broadest variation. The
 12 value of power law exponent from the fit was found to be $\alpha \approx 0.27$ with a coefficient of
 13 determination R^2 equals to 0.685. While the fairly low value of R^2 underlines the scatter
 14 around the regression line, one should interpret the α value with caution. Nevertheless, one
 15 can comment that the power law exponent is indeed closer to the theoretical value of spherical
 16 particles ($\alpha = 0.33$) than to the one of the random coil conformation of linear polymers ($\alpha =$
 17 0.5). Thus, the water-soluble polymers formed during synthesis seem to present a rather
 18 nanogel-like structure which supports the initial hypothesis of highly branched and/or
 19 crosslinked polymers with high molecular masses. In further works, SANS measurements
 20 could be envisioned to quantify the degree of branching compared to the crosslinking density.

1 Rheological and mechanical behavior of formulated microgel films

2 In the light of the interesting structure of the water-soluble polymer, the mechanical properties
3 of films composed of both microgels and the later were investigated. Five films were formed
4 following different blend compositions: 100 wt.% of microgels (classic purified film), 100
5 wt.% of WSP and 75/25, 50/50, 25/75 wt.% of microgels/WSP ratio.

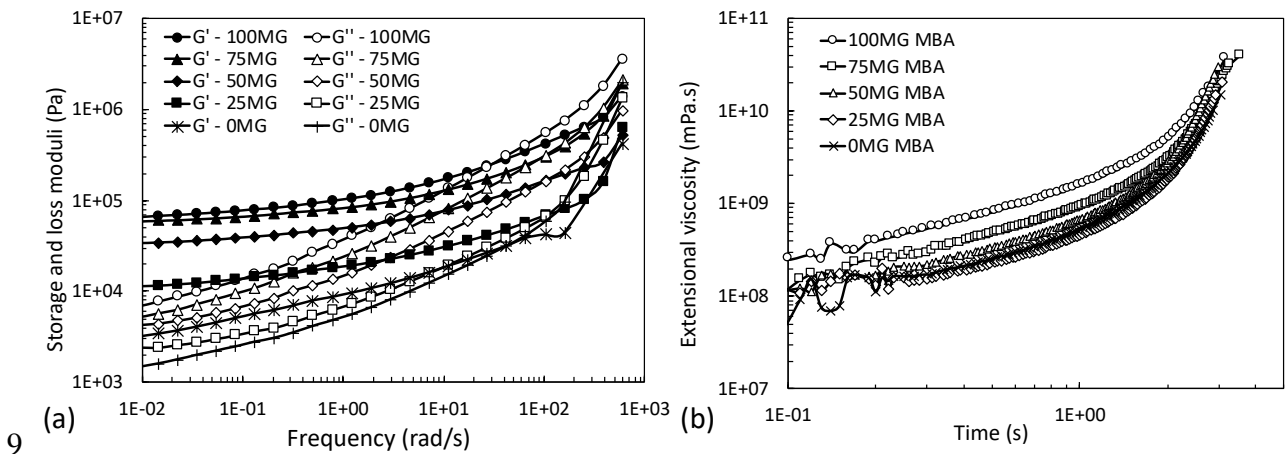
6 The inner structure of blended films was first observed with AFM performed on the surface of
7 the film cross-sections. Figures 9 (a), (b) and (c) show mappings with the height channel of
8 films composed of 25, 50 and 75 wt.% of microgels (MG), respectively. Figures 9 (d), (e) and
9 (f) show mappings with the logDMT modulus channel of the corresponding films, which
10 displays the stiffer regions in lighter colors and the softer in dark ones.



11
12 **Figure 9.** AFM (**left**) height and (**right**) LogDMT Modulus mappings of 2 mol% MBA-MG
13 films for 75% MG

14 As one expected, the modulus mappings indicate that microgels are denser than the water-
15 soluble polymer and resemble to hard spherical fillers dispersed in a soft composite matrix.
16 Microgels are quite homogeneously distributed and dispersed without any aggregates, yet no
17 structured arrangement is observed. Here again, the “donuts” structure is well observed with a
18 clear gradient in modulus and height between the cores and the shells. The looser and
19 probably more swollen shells are characterized by a greater height and a lower modulus than
20 the dense cores. Furthermore, a gradual transition is observed between the microgel shells and
21 the WSP matrix which suggests a similar structure as well as a certain interpenetration

1 between the two phases. Yet, the WSP matrix exhibits a lower modulus than the microgel
 2 shells (Figures 9 (d), (e) and (f)).
 3 The rheological behavior of blended films was investigated with small amplitude oscillatory
 4 shear measurements and extensional viscosity tests at large deformation. Figure 10 shows the
 5 storage and loss moduli *versus* frequency and the average extensional viscosity *versus* time
 6 for MBA blended films. Corresponding curves for OEGDA blended films are reported in
 7 Figure S4. The Hencky strain and the extensional viscosity, both at break, were extrapolated
 8 from the extensional curves and plotted in Figures S5.



9 **Figure 10.** (a) Storage and loss moduli *versus* frequency at 20°C (b) Average extensional
 10 viscosity *versus* time for MBA blended films at 20°C for a Hencky strain rate of 0.5 s⁻¹ with
 11 microgel and WSP contents inversely varying from 0% to 100%.
 12

13 As the microgel content decreases, one can observe the drop of both G' and G'' moduli which
 14 indicates the films become softer and more viscous. For example, the storage modulus at 0.01
 15 rad.s⁻¹ of MBA films drops from 66 kPa to 3.2 kPa for 100% microgels to 100% of WSP. The
 16 drop-in moduli arises from microgel particles being driven further away from another due the
 17 incorporation of the WSP phase. In addition, a loss of crosslinking points occurs with the
 18 rising proportion of WSPs. As a consequence, the elastic plateau of 100% MBA-WSP films is
 19 not reached because of being shifted to lower frequencies. This can be quantified by the
 20 increase of the power law exponent from the relationship $G' \propto \omega^\alpha$ where $\alpha = 0.18$ for 100%
 21 WSP compare to $\alpha = 0.06$ (near 0) for 100% MG.

22 As a direct consequence of the decrease in G' and G'' with lower microgel content, the
 23 extensional viscosity also drops with decreasing MG%. . Nonetheless, all the films
 24 demonstrate strain-hardening and break at similar strains which is surprising for films
 25 composed of a prevalent proportion of WSPs (*e.g.* 75 and 100%) (Figure S5a). Indeed, it is

1 rather uncommon to obtain such high elongation properties for a film made only from a
2 synthesis side-product since polymers rarely reach such high molecular masses and branched
3 structures. All MBA blended films demonstrate a strain at rupture close to 155 % in average
4 except the blend with 75% microgels which exhibits a higher value ($\approx 180\%$) but the
5 difference may not be significant considering the standard deviation. The preservation of the
6 elongational properties for the lower WSP content may be attributed to the presence of strain
7 hardening which is in turn a result of the branched and/or crosslinked structure of WSP. In
8 addition, we recall that the very similar chemical nature of microgels and WSP must provide
9 an excellent compatibility of the two components and strengthen their interface. MBA
10 blended films break at much higher strain than OEGDA ones, regardless of the microgel-WSP
11 composition. This was expected for blends with a prevalent proportion of microgels from the
12 results of the first section. The same observation is made for films formed from 100% of WSP
13 and the explanation lies in the structural characteristics of the latter. The analyses from size
14 exclusion chromatography have highlighted a higher molecular mass for MBA-WSP. The
15 higher molecular mass leads to higher strains at break.

16 Regarding the usefulness of self-assembled microgel films, *i.e.* raw or purified ones, they also
17 present the ability to encapsulate/release high amounts of hydrophilic/hydrophobic active
18 molecules.²⁵ Moreover, the viscoelastic properties of blended films lead to auto-adhesive
19 properties which can be piloted by the formulation.^{46,47} From the point of view of the future
20 use of these self-assembled microgel films, considering these properties, they would be used
21 as delivery patches systems or protective films for skin applications. Indeed, similar films
22 behaves as super encapsulation/release devices of active cosmetic molecules, *i.e.*
23 hydrophilic/hydrophobic either at the molecular or macromolecular states.²⁰

25 **Conclusion**

26 The relationship, which comes from analysis of thick films (about 1- 2 mm thick), between
27 the microstructure of microgels and the mechanical strength of microgel-based films was
28 successfully put into evidence thanks to dynamic mechanical measurements at low strain,
29 uniaxial tests at high deformation and AFM observations. Indeed, the looser and less
30 crosslinked structure of MBA microgels not only leads to softer films but also enhances the
31 inter-diffusion of chain at the particle interface, leading to higher strains at rupture. The
32 structural characterization of the water-soluble polymer by SEC has demonstrated higher
33 molecular masses for the polymer resulting from the MBA crosslinking than the OEGDA one.

1 This finding strengthens the idea that the looser structure of MBA microgels was due to a
2 higher portion of the crosslinker reacting with the water-soluble chains instead of the
3 microgels particles themselves. Finally, blended films were successfully formed by mixing
4 microgels and water-soluble polymers in a controlled ratio with water-soluble polymer
5 content till 100%. AFM images demonstrate that the structure of blended films resembles to
6 the one of a composite material with hard fillers (microgels) incorporated in a soft matrix
7 (water-soluble polymers). The addition of water-soluble polymer allows to vary the elastic
8 modulus of classic microgel films (G' ranging from $\approx 1 \times 10^3$ to $\approx 1 \times 10^5$ MPa) without
9 changing the elongational properties of the films. This valuable finding is attributed to the
10 branched and/or crosslinked structure of water-soluble polymers and their high compatibility
11 with microgels. As corona of dangling chains has a major impact on the properties of the film,
12 as a perspective, one can consider neutron techniques or super resolution microscopy study to
13 well reveal internal structure of the microgels.

14 Regarding the usefulness of self-assembled microgel films, *i.e.* raw or purified ones, they
15 clearly exhibit the ability for different medical applications as delivery patches systems or
16 protective films.

17

18 **Associated contents**

19 - AFM mappings of OEGDA-based microgels films

20 - Strains and extensional viscosities at rupture for different strain rates of MBA- and
21 OEGDA-based microgel films

22 - Strain at break, stress at break and fracture energy of MBA- and OEGDA-crosslinked
23 microgel films

24 - Molar mass and gyration radius as a function of elution volume of MBA and OEGDA-based
25 water-soluble polymers

26 - frequency sweep curves and average extensional viscosity curves for OEGDA blended films

27 - Hencky strain at break and extensional viscosity at break *versus* microgel for OEGDA and
28 MBA blended films.

29 **Author information**

1 Corresponding Author

2 *E-mail: christophe.derail@univ-pau.fr; Tel: +33 559407706 and laurent.billon@univ-pau.fr

3 Author Contributions

4 The manuscript was written through contributions of all authors. All authors have given
5 approval to the final version of the manuscript.

6 **Conflicts of interest**

7 The authors declared no conflict of interest.

8

9 **Acknowledgements**

10 E. Dieuzy is grateful to URGO RID, LVMH and the Région Nouvelle Aquitaine, convention
11 2016-1R10204-00007186 – THESE for her PhD financial support. This work benefits from
12 the financial support of the French National Research Agency, conventions Labcom ANR-14-
13 LAB3-0003-01 and ANR-17-LCCO-0003-01. The authors thank Pr. Brunol Grassl and Dr.
14 Nathalie Andreu for the discussion related to the SEC measurements.

15 **References**

16 (1) Steward, P. A.; Hearn, J.; Wilkinson, M. C. An Overview of Polymer Latex Film
17 Formation and Properties. *Advances in Colloid and Interface Science* **2000**, *86* (3), 195–267.

18 (2) Santos, F. D. D.; Leibler, L. Large Deformation of Films from Soft-Core/Hard-Shell
19 Hydrophobic Latices. *Journal of Polymer Science Part B: Polymer Physics* **2003**, *41* (3),
20 224–234.

21 (3) Deplace, F.; Rabjohns, M. A.; Yamaguchi, T.; Foster, A. B.; Carelli, C.; Lei, C.-H.;
22 Ouzineb, K.; Keddie, J. L.; Lovell, P. A.; Creton, C. Deformation and Adhesion of a Periodic
23 Soft–Soft Nanocomposite Designed with Structured Polymer Colloid Particles. *Soft Matter*
24 **2009**, *5* (7), 1440–1447.

25 (4) Lepizzera, S.; Lhommeau, C.; Dilger, G.; Pith, T.; Lambla, M. Film-Forming Ability
26 and Mechanical Properties of Coalesced Latex Blends. *Journal of Polymer Science Part B:*
27 *Polymer Physics* **1997**, *35* (13), 2093–2101.

28 (5) Bait, N.; Grassl, B.; Derail, C.; Benaboura, A. Hydrogel Nanocomposites as Pressure-
29 Sensitive Adhesives for Skin-Contact Applications. *Soft Matter* **2011**, *7* (5), 2025–2032.

30 (6) Oberdisse, J. Structure and Rheological Properties of Latex–Silica Nanocomposite
31 Films: Stress–Strain Isotherms. *Macromolecules* **2002**, *35* (25), 9441–9450.

32 (7) Pelton, R. Temperature-Sensitive Aqueous Microgels. *Adv Colloid Interface Sci* **2000**,
33 *85* (1), 1–33.

- 1 (8) Pelton, R. H.; Chibante, P. Preparation of Aqueous Latices with N-
2 Isopropylacrylamide. *Colloids and Surfaces* **1986**, *20* (3), 247–256.
- 3 (9) Plamper, F. A.; Richtering, W. Functional Microgels and Microgel Systems. *Acc.*
4 *Chem. Res.* **2017**, *50* (2), 131–140.
- 5 (10) Karg, M.; Pich, A.; Hellweg, T.; Hoare, T.; Lyon, L. A.; Crassous, J. J.; Suzuki, D.;
6 Gumerov, R. A.; Schneider, S.; Potemkin, Igor. I.; Richtering, W. Nanogels and Microgels:
7 From Model Colloids to Applications, Recent Developments, and Future Trends. *Langmuir*
8 **2019**, *35* (19), 6231–6255.
- 9 (11) Serpe, M. J.; Jones, C. D.; Lyon, L. A. Layer-by-Layer Deposition of
10 Thermoresponsive Microgel Thin Films. *Langmuir* **2003**, *19* (21), 8759–8764.
- 11 (12) Serpe, M. J.; Yarmey, K. A.; Nolan, C. M.; Lyon, L. A. Doxorubicin Uptake and
12 Release from Microgel Thin Films. *Biomacromolecules* **2005**, *6* (1), 408–413.
- 13 (13) Wong, J. E.; Díez-Pascual, A. M.; Richtering, W. Layer-by-Layer Assembly of
14 Polyelectrolyte Multilayers on Thermoresponsive P(NiPAM-Co-MAA) Microgel: Effect of
15 Ionic Strength and Molecular Weight. *Macromolecules* **2009**, *42* (4), 1229–1238.
- 16 (14) Li, X.; Serpe, M. J. Understanding and Controlling the Self-Folding Behavior of Poly
17 (N-Isopropylacrylamide) Microgel-Based Devices. *Advanced Functional Materials* **2014**, *24*
18 (26), 4119–4126.
- 19 (15) Hu, L.; Sarker Avijeet, K.; Islam Molla, R.; Li, X.; Lu, Z.; Serpe Michael, J. Poly (N-
20 isopropylacrylamide) Microgel-based Assemblies. *Journal of Polymer Science Part A:*
21 *Polymer Chemistry* **2013**, *51* (14), 3004–3020.
- 22 (16) Burmistrova, A.; von Klitzing, R. Control of Number Density and Swelling/Shrinking
23 Behavior of P(NIPAM–AAc) Particles at Solid Surfaces. *J. Mater. Chem.* **2010**, *20* (17),
24 3502.
- 25 (17) Nash, M. E.; Carroll, W. M.; Foley, P. J.; Maguire, G.; Connell, C. O.; Gorelov, A. V.;
26 Beloshapkin, S.; Rochev, Y. A. Ultra-Thin Spin Coated Crosslinkable Hydrogels for Use in
27 Cell Sheet Recovery—Synthesis, Characterisation to Application. *Soft Matter* **2012**, *8* (14),
28 3889.
- 29 (18) Sanzari, I.; Buratti, E.; Huang, R.; Tusan, C. G.; Dinelli, F.; Evans, N. D.;
30 Prodromakis, T.; Bertoldo, M. Poly(N-Isopropylacrylamide) Based Thin Microgel Films for
31 Use in Cell Culture Applications. *Sci Rep* **2020**, *10* (1), 6126.
- 32 (19) Zhou, J.; Wang, G.; Marquez, M.; Hu, Z. The Formation of Crystalline Hydrogel
33 Films by Self-Crosslinking Microgels. *Soft Matter* **2009**, *5* (4), 820–826.
- 34 (20) Sonzogni, A. S.; Passeggi, M. C. G.; Wedepohl, S.; Calderón, M.; Gugliotta, L. M.;
35 Gonzalez, V. D. G.; Minari, R. J. Thermoresponsive Nanogels with Film-Forming Ability.
36 *Polym. Chem.* **2018**, *9* (8), 1004–1011.
- 37 (21) Boularas, M.; Radji, S.; Gombart, E.; Tranchant, J.-F.; Alard, V.; Billon, L. Functional
38 Film by Trigger-Free Self-Assembly of Adhesive Soft Microgels at Skin Temperature.
39 *Materials & Design* **2018**, *147*, 19–27.
- 40 (22) Boularas, M.; Deniau-Lejeune, E.; Alard, V.; Tranchant, J.-F.; Billon, L.; Save, M.

- 1 Dual Stimuli-Responsive Oligo(Ethylene Glycol)-Based Microgels: Insight into the Role of
2 Internal Structure in Volume Phase Transitions and Loading of Magnetic Nanoparticles to
3 Design Stable Thermoresponsive Hybrid Microgels. *Polymer Chemistry* **2016**, 7 (2), 350–
4 363.
- 5 (23) Dieuzy, E. Relationship between Structural and Rheological Properties of Dual-
6 Stimuli Responsive Microgel Films for Cosmetic and Biomedical Applications. Thèse de
7 doctorat en Polymères, Université de Pau et des Pays de l’adour, 2019.
- 8 (24) Dieuzy, E.; Aguirre, G.; Auguste, S.; Chougrani, K.; Alard, V.; Billon, L.; Derail, C.
9 Microstructure-Driven Self-Assembly and Rheological Properties of Multi-Responsive Soft
10 Microgel Suspensions. *Journal of Colloid and Interface Science* **2021**, 581, 806–815.
- 11 (25) Aguirre, G.; Khoukh, A.; Taboada, P.; Chougrani, K.; Alard, V.; Billon, L. Smart Self-
12 Assembled Microgel Films as Encapsulating Carriers for UV-Absorbing Molecules. *Polymer*
13 *Chemistry* **2018**, 9 (10), 1155–1159.
- 14 (26) Boularas, M.; Gombart, E.; Tranchant, J.; Billon, L.; Save, M. Design of Smart
15 Oligo(Ethylene Glycol)-Based Biocompatible Hybrid Microgels Loaded with Magnetic
16 Nanoparticles. *Macromolecular Rapid Communications* **2015**, 36 (1), 79–83.
- 17 (27) Aguirre, G.; Khoukh, A.; Chougrani, K.; Alard, V.; Billon, L. Dual-Responsive
18 Biocompatible Microgels as High Loaded Cargo: Understanding of Encapsulation/Release
19 Driving Forces by NMR NOESY. *Polymer Chemistry* **2018**, 9 (6), 757–768.
- 20 (28) Ferry, J. D. *Viscoelastic Properties of Polymers*, 3d ed.; Wiley: New York, 1980.
- 21 (29) Mejia, A.; Rodriguez, L.; Schmitt, C.; Andreu, N.; Favéro, C.; Braun, O.; Dupuis, G.;
22 Deniau, E.; Reynaud, S.; Grassl, B. Synthesis and Viscosimetric Behavior of
23 Poly(Acrylamide-Co-2-Acrylamido-2-Methylpropanesulfonate) Obtained by Conventional
24 and Adiabatic Gel Process via RAFT/MADIX Polymerization. *ACS Omega* **2019**, 4 (6),
25 11119–11125.
- 26 (30) Zosel, A.; Ley, G. Influence of Crosslinking on Structure, Mechanical Properties, and
27 Strength of Latex Films. *Macromolecules* **1993**, 26 (9), 2222–2227.
- 28 (31) Pinenq, P.; Winnik, M. A.; Ernst, B.; Juhué, D. Polymer Diffusion and Mechanical
29 Properties of Films Prepared from Crosslinked Latex Particles. *Journal of Coatings*
30 *Technology* **2000**, 72 (903), 45–61.
- 31 (32) Degrandi-Contraires, E.; Udagama, R.; Bourgeat-Lami, E.; McKenna, T.; Ouzineb,
32 K.; Creton, C. Mechanical Properties of Adhesive Films Obtained from PU–Acrylic Hybrid
33 Particles. *Macromolecules* **2011**, 44 (8), 2643–2652.
- 34 (33) Udagama, R.; Degrandi-Contraires, E.; Creton, C.; Graillat, C.; McKenna, T. F. L.;
35 Bourgeat-Lami, E. Synthesis of Acrylic–Polyurethane Hybrid Latexes by Miniemulsion
36 Polymerization and Their Pressure-Sensitive Adhesive Applications. *Macromolecules* **2011**,
37 44 (8), 2632–2642.
- 38 (34) Ward, I. M.; Sweeney, J. *An Introduction to the Mechanical Properties of Solid*
39 *Polymers*, 2nd ed.; Wiley: Chichester, West Sussex, England, 2004.
- 40 (35) Sentmanat, M.; Wang, B. N.; McKinley, G. H. Measuring the Transient Extensional
41 Rheology of Polyethylene Melts Using the SER Universal Testing Platform. *Journal of*

- 1 *Rheology* **2005**, 49 (3), 585–606.
- 2 (36) Paillet, S.; Roncin, A.; Clisson, G.; Pembouong, G.; Billon, L.; Derail, C.; Save, M.
3 Combination of Nitroxide-mediated Polymerization and SET-LRP for the Synthesis of High
4 Molar Mass Branched and Star-branched Poly(N-butyl Acrylate) Characterized by Size
5 Exclusion Chromatography and Rheology. *Journal of Polymer Science Part A: Polymer*
6 *Chemistry* **2012**, 50 (14), 2967–2979.
- 7 (37) Stange, J.; Münstedt, H. Effect of Long-Chain Branching on the Foaming of
8 Polypropylene with Azodicarbonamide. *Journal of Cellular Plastics* **2006**, 42 (6), 445–467.
- 9 (38) Ajji, A.; Sammut, P.; Huneault, M. A. Elongational Rheology of LLDPE / LDPE
10 Blends. *Journal of Applied Polymer Science* **2003**, 88 (14), 3070–3077.
- 11 (39) Tabatabaei Seyed, H.; Carreau Pierre, J.; Ajji, A. Rheological Properties of Blends of
12 Linear and Long-chain Branched Polypropylenes. *Polymer Engineering & Science* **2009**, 50
13 (1), 191–199.
- 14 (40) Yamaguchi, M.; Suzuki, K.-I.; Maeda, S. Enhanced Strain Hardening in Elongational
15 Viscosity for HDPE/Crosslinked HDPE Blend. I. Characteristics of Crosslinked HDPE.
16 *Journal of Applied Polymer Science* **2002**, 86 (1), 73–78.
- 17 (41) Wu, C.; Zhou, S. Laser Light Scattering Study of the Phase Transition of Poly(N-
18 Isopropylacrylamide) in Water. 1. Single Chain. *Macromolecules* **1995**, 28 (24), 8381–8387.
- 19 (42) Mourran, A.; Wu, Y.; Gumerov, R. A.; Rudov, A. A.; Potemkin, I. I.; Pich, A.; Möller,
20 M. When Colloidal Particles Become Polymer Coils. *Langmuir* **2016**, 32 (3), 723–730.
- 21 (43) Siviour, C. R.; Jordan, J. L. High Strain Rate Mechanics of Polymers: A Review. *J.*
22 *dynamic behavior mater.* **2016**, 2 (1), 15–32.
- 23 (44) Cai, T.; Wang, G.; Thompson, S.; Marquez, M.; Hu, Z. Photonic Hydrogels with
24 Poly(Ethylene Glycol) Derivative Colloidal Spheres as Building Blocks. *Macromolecules*
25 **2008**, 41 (24), 9508–9512.
- 26 (45) Yu, B.; Kang, S.-Y.; Akthakul, A.; Ramadurai, N.; Pilkenton, M.; Patel, A.; Nashat,
27 A.; Anderson, D. G.; Sakamoto, F. H.; Gilchrest, B. A.; Anderson, R. R.; Langer, R. An
28 Elastic Second Skin. *Nature Materials* **2016**, 15 (8), 911–918.
- 29 (46) Renvoise, J.; Burlot, D.; Marin, G.; Derail, C. Peeling of PSAs on Viscoelastic
30 Substrates: A Failure Criterion. *The Journal of Adhesion* **2007**, 83 (4), 403–416.
- 31 (47) Renvoise, J.; Burlot, D.; Marin, G.; Derail, C. Adherence Performances of Pressure
32 Sensitive Adhesives on a Model Viscoelastic Synthetic Film: A Tool for the Understanding of
33 Adhesion on the Human Skin. *Int J Pharm* **2009**, 368 (1–2), 83–88.
- 34 (48) Kalra, A.; Lowe, A.; Al-Jumaily, A. Mechanical Behaviour of Skin: A Review. *J*
35 *Material Sci Eng* **2016**, 5 (4).
- 36 (49) Ní Annaidh, A.; Bruyère, K.; Destrade, M.; Gilchrist, M. D.; Otténio, M.
37 Characterization of the Anisotropic Mechanical Properties of Excised Human Skin. *Journal of*
38 *the Mechanical Behavior of Biomedical Materials* **2012**, 5 (1), 139–148.
- 39 (50) Gallagher, A.; Ní Annaidh, A.; Bruyère-Garnier, K.; et al. Dynamic Tensile Properties

- 1 of Human Skin; International Research Council on the Biomechanics of Injury, 2012; pp 12–
2 14.
- 3 (51) Lepizzera, S.; Scheer, M.; Fond, C.; Pith, T.; Lambla, M.; Lang, J. Coalesced
4 Core/Shell Latex Films under Elongation Imaged by Atomic Force Microscopy.
5 *Macromolecules* **1997**, *30* (25), 7953–7957.
- 6 (52) Lepizzera, S.; Pith, T.; Fond, C.; Lambla, M. Mechanical Behavior at Finite Strain of
7 Coalesced Core/Shell Latex Films. *Macromolecules* **1997**, *30*, 7945–7952.
- 8 (53) Bitar, A.; Fessi, H.; Elaissari, A. Synthesis and Characterization of Thermally and
9 Glucose-Sensitive Poly N-Vinylcaprolactam-Based Microgels. *J Biomed Nanotechnol* **2012**, *8*
10 (5), 709–719.
- 11 (54) Kratochvíl, P.; Netopilík, M. The Effect of Nanoparticle Nonuniformity on the Ratio
12 of Gyration and Hydrodynamic Radiuses. *International Journal of Polymer Analysis and*
13 *Characterization* **2017**, *22* (2), 112–117.

14

